A Fast and Robust Diagnostic Method for Multiple Open-Circuit Faults of Voltage-Source Inverters Through Line Voltage Magnitudes Analysis

Xun Wu, Chun-Yang Chen, Te-Fang Chen, Shu Cheng, Zhi-Hong Mao, *Senior Member, IEEE*, Tian-Jian Yu, and Kaidi Li

***Abstract*—In this article, a fast and robust diagnostic method for multiple open-circuit (OC) faults is presented for voltage-source inverters. Only two line voltages are used as diagnosis variables, which is economic, simple, and can reduce the influence caused by the failure rate of information sources. Possible magnitudes of these line voltage vectors are characterized in detail both for the healthy and faulty operations. Then, several voltage features are extracted for diagnosis. Single-switch open-circuit faults and double-switch open-circuit faults can be accurately and quickly located through the proposed method. The fastest diagnostic process can be finished in 1/20 of the fundamental period. The diagnostic results of the proposed method are not affected by certain load OC faults, which may lead to false diagnosis of the existing methods. Moreover, the proposed method is robust to different control strategies, filter components, and carrier frequencies. Experiments are carried out on a dSPACE platform, and the effectiveness of the proposed method is verified.**

***Index Terms*—Fault diagnosis, fault location, inverters.**

I. Introduction

THREE-PHASE inverters are widely utilized in various applications, such as uninterruptible power system, active power filters, and renewable energy conversion systems. Although inverters have excellent performance of energy saving and control, they may suffer critical failures when exposed to high stress and hard environment conditions. Generally, the main failures of inverters are classified as short-circuit faults and open-circuit (OC) faults [1]. Short-circuit faults are more destructive than OC faults and may lead to the shutdown of the system immediately. As a result, they are usually prevented by introducing protection layers. Although OC fault is not as dangerous as short-circuit fault, if it remains as is for an extended period of time, it will eventually cause secondary damages leading to the system shutdown and high repair costs. A number of fault-tolerant control strategies [2]–[8] have been proposed to control and prevent the spread of these failures; however, the premise to implement these strategies is the fast fault diagnosis.

Currently, inverter fault diagnosis is still a research hotspot, concerning the reliability and maintainability. A large number of studies have been carried out on the OC fault diagnosis of inverters. The existing methods can be divided into three groups according to the deployed diagnosis variables.

1) Current-based diagnostic methods [8]–[18]. These methods usually detect OC faults directly via three-phase currents, i_q/i_d, or bus currents. Current pattern recognition [9]–[11] is one of the most popular techniques for fault location. Faults can be diagnosed by intelligent algorithms or using only the radius and angle of the current pattern. Additionally, faults can be diagnosed by harmonics, average, and root mean square currents as well [8], [12], [14]–[17]. Most current-based methods focus on single-switch open-circuit (SSOC) fault diagnosis; a few researchers [15]–[18] also studied multiswitch OC fault diagnosis. Although current detection is convenient in many diagnosis occasions, researchers have to adopt more strategies to minimize the influence of load variation, increasing the complexity of the diagnosis algorithms. Moreover, most of the methods based on current detection may not be applicable if OC faults occur at the load side, because these faults can lead to the output current interruption. This problem has not been referred to and studied in existing diagnosis methods for inverter OC faults.
2) Voltage-based diagnostic methods [19]–[28]. There are also a number of fault diagnosis methods based on the voltage detection. Line voltages and pole voltages are mainly utilized as diagnosis variables. Faults are usually diagnosed through the comparison of the measured and ideal values [19], [20] and switching function models [21]–[23]. These methods are able to locate OC faults accurately; however, control signals are indispensable variables for diagnosis. Considering the reliability of the systems, they may not be applicable to existing inverters without any modification. The combination of the principle component analysis and the multiclass relevance vector machine is an

Manuscript received March 3, 2019; revised April 27, 2019 and August 3, 2019; accepted August 31, 2019. Date of publication September 15, 2019; date of current version February 11, 2020. This work was supported in part by the National Key R&D Program of China under Grants 2016YFB1200401, 2017YFB1201302-13, and 2017YFB1200902-11, and in part by China Scholarship Council under Grant 201806370150. Recommended for publication by Associate Editor B. Mirafzal. *(Corresponding author: Tian-Jian Yu.)*

X. Wu, C.-Y. Chen, T.-F. Chen, S. Cheng, T.-J. Yu, and K. Li are with the Department of Traffic and Transportation Engineering, Central South University, Changsha 12570, China (e-mail: 309931624@qq.com; cychen999@csu.edu.cn; ctfcyt@163.com; 6409020@qq.com; 250486154@qq.com; 17504 5912@qq.com).

Z.-H. Mao is with the Department of Electrical and Computer Engineering, University of Pittsburgh, Pittsburgh, PA 15261 USA (e-mail: zhm4@pitt.edu).

Color versions of one or more of the figures in this article are available online at http://ieeexplore.ieee.org.

Digital Object Identifier 10.1109/TPEL.2019.2941480

effective tool for cascaded H-bridge multilevel inverter diagnosis, and three-phase voltages are required [25]. Bayesian network [26] and neural networks [27], [28] are also used for diagnosis. But the parameter selection of intelligent algorithms is an intractable problem when these methods are applied to other different systems. Extra time is required for adjusting the models and seeking the optimal structures. Moreover, intelligent algorithms that require training samples are also inappropriate for the diagnosis because it is difficult to obtain a large number of real and universal samples, especially in some important applications that require high reliability.

3) Multisource information based diagnostic methods [29]–[46]. Faults can be diagnosed by combining information, such as currents and speed [31]–[33], currents and voltages [35]–[40], currents and control signals [44], [45], and voltages and control signals [46]. Several diagnosis methods, such as [32] and [44], are able to locate double-switch open-circuit (DSOC) faults. Although multisource information based diagnosis methods are able to provide more comprehensive analysis of OC faults through information of different aspects, the reliability of themselves is still a question. Generally, one may think more information means higher reliability. This may not be true as expected when considering the failure rate of information sources. Studies have shown that sensors in poor working conditions are also potential fault points [14], [47], [48]. Assuming that all resources are properly used, and information sources have the same failure rate. It can be calculated that the rate of overlook or false diagnosis of the method using three information sources is larger than that using only two information sources. Therefore, more information sources do not necessarily mean higher diagnostic reliability; they may even increase the error rate. Of course, some strategies can be used to enhance the reliability while using more date sources, but, on the other hand, that will definitely increase the system cost and complexity.

In this article, a fast, robust, simple, and low-cost fault diagnosis method is proposed for single- and double-switch OC faults in voltage-source inverters. The proposed method has several advantages. The OC faults can be accurately located by the proposed method within 1/20 of the fundamental period in some cases. The fault diagnosis results are immune to certain load OC faults, which may lead to false diagnosis of the existing methods. The proposed method is also robust to different control strategies, filter components, and carrier frequencies. Moreover, neither control signals nor other modifications are required in the proposed method. Only two line voltage sensors are used for diagnosis purpose, which is simple, reliable, and economic, and can be easily implemented in both existing and newly built inverters.

The rest of this article is organized as follows: Section II analyzes the health operation and fault operation of an inverter on a passenger train, respectively. Section III describes the proposed diagnostic method. Section IV presents the experimental results of the proposed method. Section V compares the proposed method with existing diagnosis methods. Section VI summarizes the article.

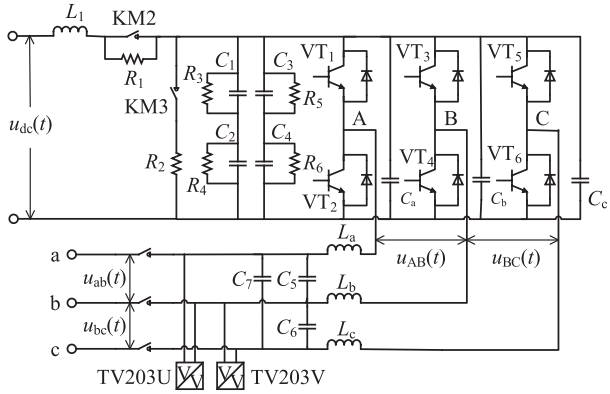

Fig. 1. Main circuit of an inverter on a passenger train.

II. Inverter and Operation Analysis

A. Operational Principle of the Inverter

An inverter on a passenger train is utilized as an example for analysis, and the main circuit is shown in Fig. 1. The input voltage $u_{\rm dc}(t)$ is 600 VDC; the outputs are three-phase 380 V/ 50 Hz. Sinusoidal pulse width modulation (SPWM) is adopted. L_1 and R_1 are precharged circuits. KM2 is turned ON when the precharge is completed. C_1–C_4 and R_3–R_6 are dc-side components to stabilize the input voltage. KM3 and R_2 are discharge circuits. When the inverter is shut down, KM3 is turned ON and the energy in the dc-link capacitors is released. $\rm VT_1$–$\rm VT_6$ are insulated gate bipolar transistors with corresponding antiparallel diodes. C_a–C_c are three-phase inductance capacitors. L_a–L_c are three-phase filter inductances. C_5–C_6 are three-phase filter capacitors. Output voltages $u_{ab}(t)$ and $u_{bc}(t)$ are measured by voltage sensors TV203U and TV203V, respectively.

Usually, output voltages can be given as

$$\begin{cases} u_{ab}(t) = U_m \sin(\omega t) \\ u_{bc}(t) = U_m \sin(\omega t + \varphi) \\ u_{ca}(t) = U_m \sin(\omega t + 2\varphi) \end{cases} \tag{1}$$

where U_m is the amplitude, ω is the angular frequency of modulation wave, and φ is the phase angle –2π/3.

The ratio of $u_{bc}(t)$ and $u_{ab}(t)$ is

$$r(t) = \frac{u_{bc}(t)}{u_{ab}(t)} = \frac{\sin(\omega t + \varphi)}{\sin(\omega t)} = \sin(\varphi)\cot(\omega t) + \cos(\varphi). \tag{2}$$

It can be seen that the ratio changes periodically in the form of cotangent. The period is equal to that of the output line voltages.

B. Analysis of Fault Operations

Under fault conditions, the output voltages can be indirectly analyzed through voltages $u_{\rm AB}(t)$, $u_{\rm BC}(t)$, and $u_{\rm CA}(t)$, because

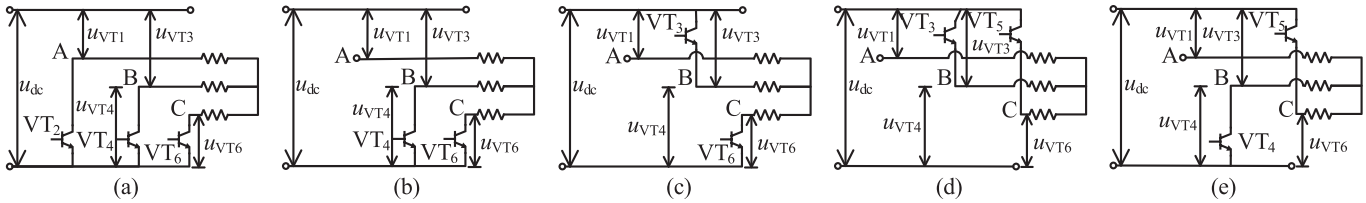

Fig. 2. Equivalent circuits when VT_1 fails. (a) $tr_A(t) = tr_B(t) = tr_C(t) = 0$. (b) $tr_A(t) = 1$ and $tr_B(t) = tr_C(t) = 0$. (c) $tr_A(t) = tr_B(t) = 1$ and $tr_C(t) = 0$. (d) $tr_A(t) = tr_B(t) = tr_C(t) = 1$. (e) $tr_A(t) = 1$, $tr_B(t) = 0$, and $tr_C(t) = 1$.

they are easier to calculate. In the analysis, we assume that the inverter runs with pure resistive load to simplify it.

Voltages $u_{AB}(t)$, $u_{BC}(t)$, and $u_{CA}(t)$ can be obtained by Kirchhoff's law

$$\begin{cases} u_{AB}(t) = u_{dc} - u_{VT1}(t) - u_{VT4}(t) \\ u_{BC}(t) = u_{dc} - u_{VT3}(t) - u_{VT6}(t) \\ u_{CA}(t) = u_{dc} - u_{VT5}(t) - u_{VT2}(t) \end{cases} \tag{3}$$

where $u_{VT1}(t)$–$u_{VT6}(t)$ are voltages of VT_1–VT_6, respectively.

If an OC fault occurs, the line voltages will have the obvious fault features in a time zone, in which the control signal of the switch has a high duty ratio. The time zone appears periodically in each period, and it is the best time for fault analysis. Different OC faults have different time zones. The time zones of OC faults in a period are calculated according to the modulation waves and the conduction time of the switches

Z_1 of VT_1 OC fault: $\pi/6 < \omega t < 5\pi/6$.
Z_2 of VT_2 OC fault: $7\pi/6 < \omega t < 11\pi/6$.
Z_3 of VT_3 OC fault: $5\pi/6 < \omega t < 3\pi/2$.
Z_4 of VT_4 OC fault: $0 < \omega t < \pi/2$ and $11\pi/6 < \omega t < 2\pi$.
Z_5 of VT_5 OC fault: $0 < \omega t < \pi/6$ and $3\pi/2 < \omega t < 2\pi$.
Z_6 of VT_6 OC fault: $\pi/2 < \omega t < 7\pi/6$.

When VT_1 OC fault occurs, control signals $tr_A(t)$–$tr_C(t)$ have five different combinations in Z_1, as shown in Fig. 2. The upper arm is activated when the control signal is 1; the lower arm is activated when the control signal is 0. Voltages $u_{AB}(t)$ and $u_{BC}(t)$ in Z_1 can be calculated as follows.

When $tr_A(t) = tr_B(t) = tr_C(t) = 0$, then, $u_{VT1} = u_{VT3} = u_{dc}$, $u_{VT4} = u_{VT6} = 0$, $u_{AB} = u_{BC} = 0$. When $tr_A(t) = 1$, $tr_B(t) = tr_C(t) = 0$, then, $u_{VT1} = u_{VT3} = u_{dc}$, $u_{VT4} = u_{VT6} = 0$, $u_{AB} = u_{BC} = 0$. When $tr_A(t) = tr_B(t) = 1$, $tr_C(t) = 0$, then, $u_{VT1} = u_{dc}/2$, $u_{VT3} = u_{VT6} = 0$, $u_{VT4} = u_{dc}$, $u_{AB} = -u_{dc}/2$, $u_{BC} = u_{dc}$. When $tr_A(t) = tr_B(t) = tr_C(t) = 1$, then, $u_{VT1} = u_{VT3} = 0$, $u_{VT4} = u_{VT6} = u_{dc}$, $u_{AB} = u_{BC} = 0$. When $tr_A(t) = tr_C(t) = 1$, $tr_B(t) = 0$, then, $u_{VT1} = u_{dc}/2$, $u_{VT3} = u_{VT6} = u_{dc}$, $u_{VT4} = 0$, $u_{AB} = u_{dc}/2$, $u_{BC} = -u_{dc}$.

The rectangular wave values of u_{AB} and u_{BC} during Z_1 are listed in Table I. It can be observed that the value of $u_{BC}(t)/u_{AB}(t)$ is –2 during this period. Because the parameters of the three-phase filter components are consistent, the filter transfer functions in the three phases are the same as well. The value of $u_{bc}(t)/u_{ab}(t)$ is the same as that of $u_{BC}(t)/u_{AB}(t)$, according to the linear relationship.

TABLE I
RECTANGULAR WAVE VALUES OF VT_1 OC FAULT

Fault switch	$tr_A(t)$	$tr_B(t)$	$tr_C(t)$	$u_{AB}(t)$	$u_{BC}(t)$
VT_1	0	0	0	0	0
	1	0	0	0	0
	1	1	0	$-u_{dc}/2$	u_{dc}
	1	1	1	0	0
	1	0	1	$u_{dc}/2$	$-u_{dc}$

When VT_2 OC fault occurs, control signals $tr_A(t)$–$tr_C(t)$ have five different combinations in Z_2, as shown in Fig. 3. Voltages $u_{AB}(t)$ and $u_{BC}(t)$ in Z_2 can be calculated as follows.

When $tr_A(t) = tr_B(t) = tr_C(t) = 0$, then $u_{VT1} = u_{VT3} = u_{dc}$, $u_{VT4} = u_{VT6} = 0$, $u_{AB} = u_{BC} = 0$. When $tr_A(t) = tr_B(t) = 0$, $tr_C(t) = 1$, then, $u_{VT1} = u_{dc}/2$, $u_{VT3} = u_{VT6} = u_{dc}$, $u_{VT4} = 0$, $u_{AB} = u_{dc}/2$, $u_{BC} = -u_{dc}$. When $tr_A(t) = 0$, $tr_B(t) = tr_C(t) = 1$, then, $u_{VT1} = u_{VT3} = 0$, $u_{VT4} = u_{VT6} = u_{dc}$, $u_{AB} = u_{BC} = 0$. When $tr_A(t) = tr_B(t) = tr_C(t) = 1$, then, $u_{VT1} = u_{VT3} = 0$, $u_{VT4} = u_{VT6} = u_{dc}$, $u_{AB} = u_{BC} = 0$. When $tr_A(t) = tr_C(t) = 0$, $tr_B(t) = 1$, then, $u_{VT1} = u_{dc}/2$, $u_{VT3} = u_{VT6} = 0$, $u_{VT4} = u_{dc}$, $u_{AB} = -u_{dc}/2$, $u_{BC} = u_{dc}$.

The rectangular wave values of u_{AB} and u_{BC} during Z_2 are listed in Table II. The ratios of both $u_{BC}(t)/u_{AB}(t)$ and $u_{bc}(t)/u_{ab}(t)$ are –2.

The voltage values can be obtained in the same way when faults occur in other phases. Table III lists the rectangular wave values of u_{AB} and u_{BC} during the time zones of other OC faults. When the b-phase fails, The ratios of both $u_{BC}(t)/u_{AB}(t)$ and $u_{bc}(t)/u_{ab}(t)$ are 1. When c-phase fails, The ratios of both $u_{BC}(t)/u_{AB}(t)$ and $u_{bc}(t)/u_{ab}(t)$ are –1/2.

It is noted that any factor that causes the two voltages to change in the same proportion will not affect the ratio of the two voltages, for example, the replacement of qualified filter components.

III. PROPOSED DIAGNOSIS METHOD

The fault phase can be accurately determined according to the voltage ratio, which is one of the key parts of the diagnosis. But it is difficult to distinguish whether the fault is in the upper arm or lower arm of the phase with the voltage ratio alone. Thus, the voltage difference is also used as the diagnosis variable in the proposed method, and the specific location of the fault can be finally identified.

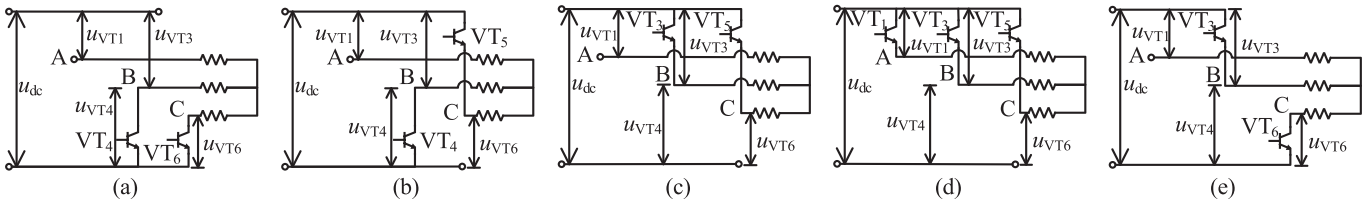

Fig. 3. Equivalent circuits when VT_2 fails. (a) $tr_A(t) = tr_B(t) = tr_C(t) = 0$. (b) $tr_A(t) = tr_B(t) = 0$ and $tr_C(t) = 1$. (c) $tr_A(t) = 0$ and $tr_B(t) = tr_C(t) = 1$. (d) $tr_A(t) = tr_B(t) = tr_C(t) = 1$. (e) $tr_A(t) = 0$, $tr_B(t) = 1$, and $tr_C(t) = 0$.

TABLE II
RECTANGULAR WAVE VALUES OF VT_2 OC FAULT

Fault switch	$tr_A(t)$	$tr_B(t)$	$tr_C(t)$	$u_{AB}(t)$	$u_{BC}(t)$
VT_2	0	0	0	0	0
	0	0	1	$u_{dc}/2$	$-u_{dc}$
	0	1	1	0	0
	1	1	1	0	0
	0	1	0	$-u_{dc}/2$	u_{dc}

TABLE III
RECTANGULAR WAVE VALUES OF OTHER OC FAULTS

Fault switch	$tr_A(t)$	$tr_B(t)$	$tr_C(t)$	$u_{AB}(t)$	$u_{BC}(t)$
VT_3	0	0	0	0	0
	0	1	0	0	0
	0	1	1	$-u_{dc}/2$	$-u_{dc}/2$
	1	1	1	0	0
	1	1	0	$u_{dc}/2$	$u_{dc}/2$
VT_4	0	0	0	0	0
	0	0	1	$-u_{dc}/2$	$-u_{dc}/2$
	1	0	1	0	0
	1	1	1	0	0
	1	0	0	$u_{dc}/2$	$u_{dc}/2$
VT_5	0	0	0	0	0
	0	0	1	0	0
	0	1	1	$-u_{dc}$	$u_{dc}/2$
	1	1	1	0	0
	1	0	1	u_{dc}	$-u_{dc}/2$
VT_6	0	0	0	0	0
	1	0	0	u_{dc}	$-u_{dc}/2$
	1	1	0	0	0
	1	1	1	0	0
	0	1	0	$-u_{dc}$	$u_{dc}/2$

The proposed method includes three parts: the fault phase determination, the effective diagnosis confirmation, and the fault switch location. The fault is detected when the ratio is a constant in a short period of time, and the fault phase is determined by the ratio. Then, a simple voltage monitoring algorithm is activated to prevent false diagnosis. By identifying the voltage difference, the fault switch is located. It is known that each of SSOC faults has a distinctive time zone for diagnosis. Moreover, any two time zones do not overlap completely. This means the DSOC faults can be divided into two SSOC faults, and the two faults can be separately located through the nonoverlapping parts of the time zones. If the diagnosis method goes on, the second fault switch will be located. Therefore, the DSOC faults diagnosis is achieved.

A. Fault Phase Determination

Line voltages u_{ab} and u_{bc} are sampled for the ratio calculation. Here, two queues are used to store the sampling points of the two line voltages. The length of each queue is n ($n \in \mathbf{N}^+$). Theoretically, n is greater than 1, and the time span of all sampling points should not exceed the minimum interval for fault diagnosis. At time k ($k \geq n$), we have $u_{ab}[k]$, $u_{ab}[k-1]$, …, $u_{ab}[k-n+1]$, and $u_{bc}[k]$, $u_{bc}[k-1]$, …, $u_{bc}[k-n+1]$. Thus, the ratio in the discrete form can be obtained

$$r\,[k] = \frac{u_{bc}\,[k]}{u_{ab}\,[k]}. \tag{4}$$

However, the accuracy of the calculation is not high, especially in the condition that the absolute value of the divisor is much smaller than that of the dividend. Therefore, we hope to utilize more information in the ratio calculation to ensure the accuracy, and the improved algorithm for the ratio calculation is given

$$r_u\,[k] = \frac{u_{bc}\,[k] - u_{bc}\,[k-1]}{u_{ab}\,[k] - u_{ab}\,[k-1]}. \tag{5}$$

According to the operation analysis, the calculated ratios will not converge to a constant if the inverter is healthy. When the calculated ratios are close to any constant of –2, 1, and –1/2 in a period of time, then, the fault is detected and the fault phase is determined. Because line voltages u_{ab} and u_{bc} may not strictly follow the relationship described by (4) or (5) under faulty operations, the fault may not be detected even if the fault happens. Thus, a threshold is needed for the fault phase detection considering the interference and errors. This can be given as follows: Equation (6) shown at the bottom of this page, where $\mathbf{R}_u$ is the assemblage of the calculated ratios, $\mathbf{R}_u = \{r_u[k], r_u[k-1], \ldots, r_u[k-n+2]\}$. The threshold δ

$$\begin{cases} \mathbf{R}_u \subset [\tan[\arctan(-2) - \delta], \tan[\arctan(-2) + \delta]] & \text{a - phase failure} \\ \mathbf{R}_u \subset [\tan[\arctan(1) - \delta], \tan[\arctan(1) + \delta]] & \text{b - phase failure} \\ \mathbf{R}_u \subset [\tan[\arctan(-1/2) - \delta], \tan[\arctan(-1/2) + \delta]] & \text{c - phase failure} \end{cases} \tag{6}$$

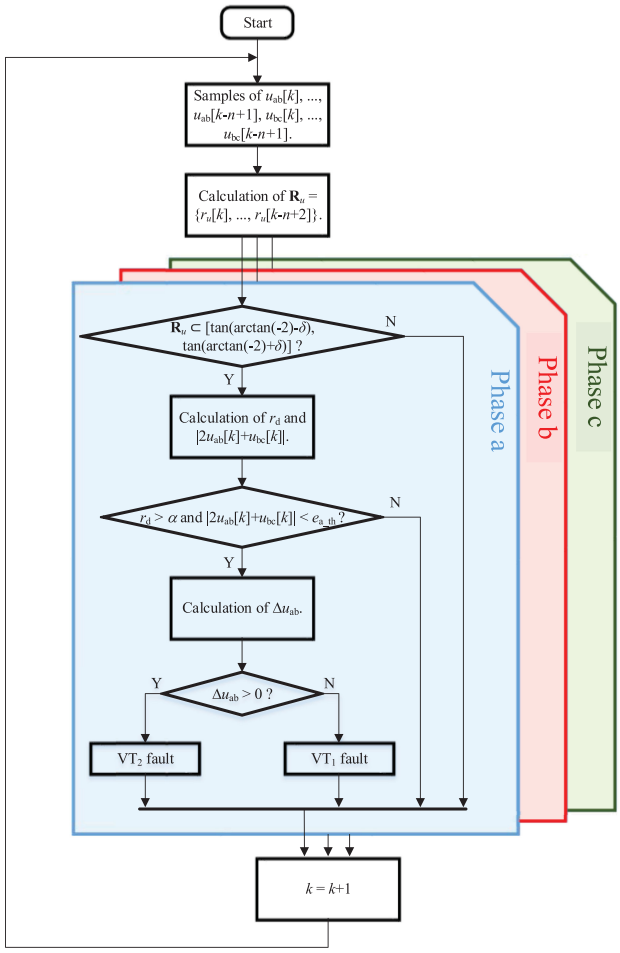

Fig. 4. Diagnosis process of OC faults in a-phase.

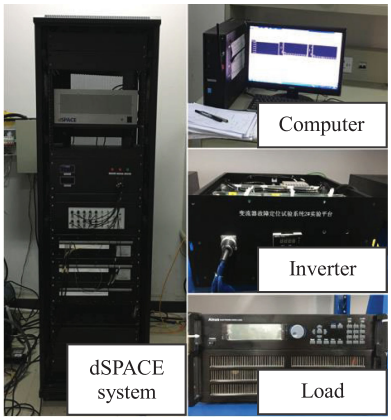

Fig. 5. Experimental system.

is a positive value, which is less than half of the difference between arctan(–1/2) and arctan(–2). In other words, δ should be less than 18.43°. Otherwise, the ranges for a-phase failure detection and c-phase failure detection will be overlapped, leading to the contradictory of (6). Generally, δ is suggested to be closed to its maximum, because it can tolerate the worse influence of noise and interference on the calculated ratios. Here, $\delta = 15°$.

TABLE IV
KEY PARAMETERS OF THE PROTOTYPE

Parameters	Values	Parameters	Values
VT_1–VT_6	IKW40N120T2	Input	600 VDC
Trigger IC	1ED020I12FA	Outputs	Three-phase 380 VAC
		Load	9 kW
Controller	f_m = 50 Hz	Filter components	$L_a = L_b = L_c$ = 4.5 mH
	f_c = 1 kHz		$C_5 = C_6 = C_7$ = 90 μF
	Modulation index is 0.8	Diagnosis system	Sampling interval is 100 μs
			n = 6

B. *Effective Diagnosis Confirmation*

Under faulty operation, the ratio calculation might be inaccurate when the two line voltages decrease to low values. These errors may lead to the false detection. Therefore, a precise geometric constraint is given to prevent the division of two near-zero numbers

$$\begin{cases} r_d > \alpha \\ r_d = \dfrac{(u_{ab}[k] - u_{bc}[k])^2 (1+\cos\varphi)}{2U_m^2 \sin^2\varphi} \\ \qquad + \dfrac{(u_{ab}[k] + u_{bc}[k])^2 (1-\cos\varphi)}{2U_m^2 \sin^2\varphi}. \end{cases} \tag{7}$$

The constrain means that $u_{ab}[k]$ and $u_{bc}[k]$ under faulty operations are effective only when r_d is greater than a positive value α. The derivation of this constrain is given as follows.

Derivation: First, the equation of voltages u_{ab} and u_{bc} is required. The product of ω and t is obtained from (1)

$$\begin{cases} \omega t = \frac{\pi}{2} - \cos^{-1}\left(\frac{u_{ab}}{U_m}\right) \\ \omega t = \sin^{-1}\left(\frac{u_{bc}}{U_m}\right) - \varphi. \end{cases} \tag{8}$$

Cancel ωt and combine the two equations, we have

$$\varphi + \frac{\pi}{2} = \cos^{-1}\left(\frac{u_{ab}}{U_m}\right) + \sin^{-1}\left(\frac{u_{bc}}{U_m}\right). \tag{9}$$

Sine of (9) is

$$\cos(\varphi) = \sin\left[\cos^{-1}\left(\frac{u_{ab}}{U_m}\right)\right] \cdot \cos\left[\sin^{-1}\left(\frac{u_{bc}}{U_m}\right)\right] + \frac{u_{ab}}{U_m} \cdot \frac{u_{bc}}{U_m}. \tag{10}$$

It can be expressed as

$$\cos(\varphi) - \frac{u_{ab}}{U_m} \cdot \frac{u_{bc}}{U_m} = \sqrt{\left[1 - \left(\frac{u_{ab}}{U_m}\right)^2\right] \cdot \left[1 - \left(\frac{u_{bc}}{U_m}\right)^2\right]}. \tag{11}$$

Thus, the relationship between u_{ab} and u_{bc} can be obtained by (11)

$$u_{ab}^2 + u_{bc}^2 - 2\cos(\varphi) u_{ab} u_{bc} - U_m^2 \sin^2(\varphi) = 0. \tag{12}$$

It is noted that ωt in (8) actually has two solutions but the derivations of (12) are the same.

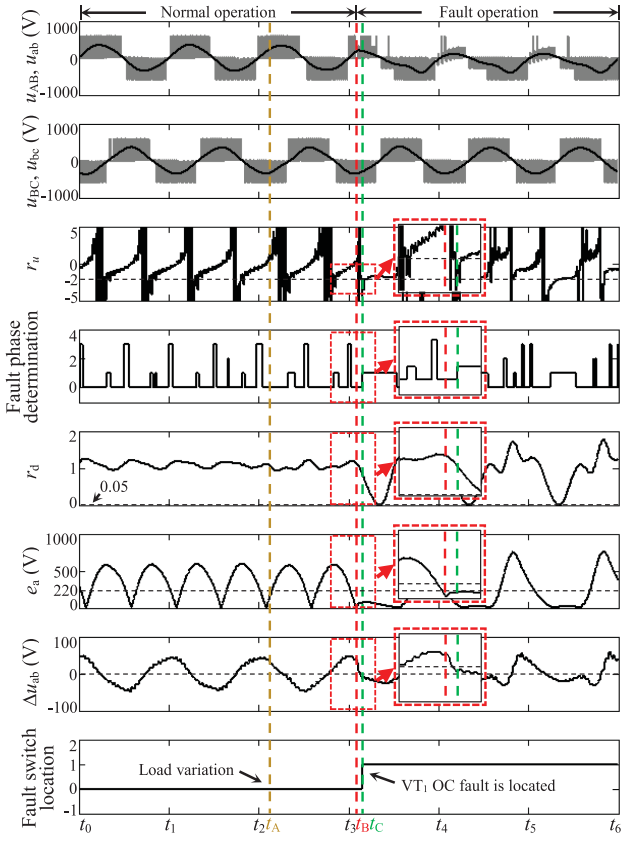

Fig. 6. Diagnosis of VT_1 OC fault.

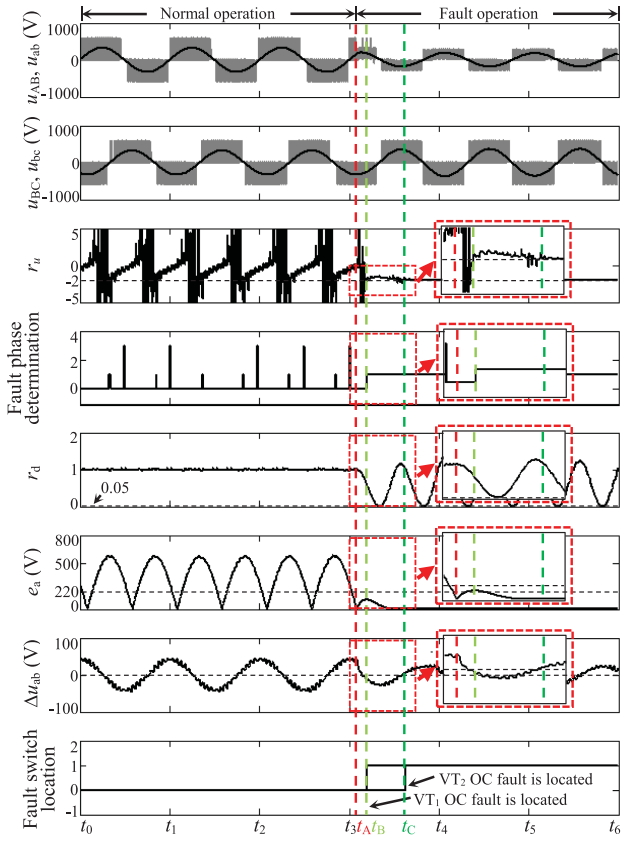

Fig. 7. Diagnosis of VT_1 and VT_2 OC faults.

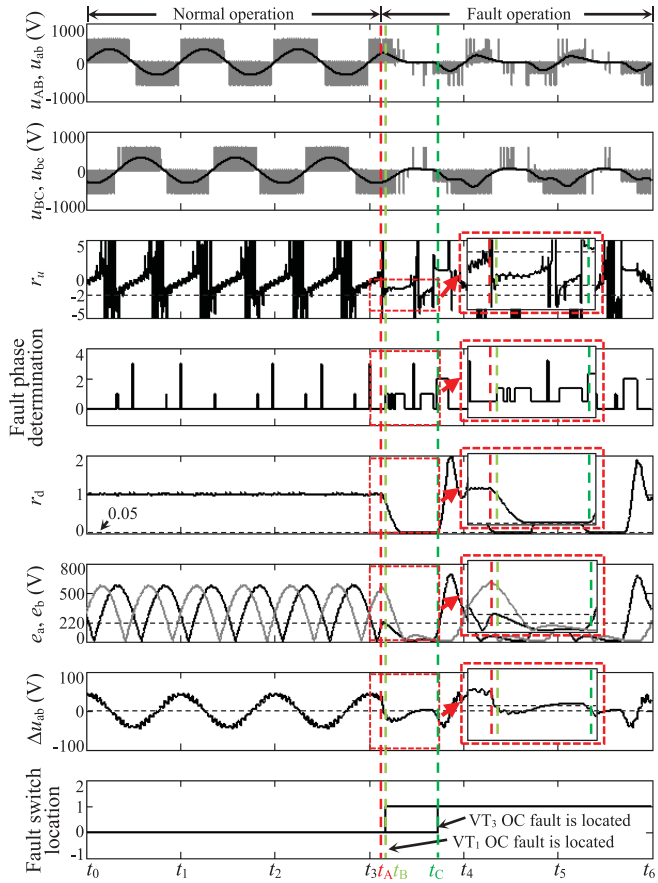

Fig. 8. Diagnosis of VT_1 and VT_3 OC faults.

Define

$$\begin{cases} u_{ab} = \frac{\sqrt{2}}{2}\left(u'_{ab} + u'_{bc}\right) \\ u_{bc} = \frac{\sqrt{2}}{2}\left(u'_{bc} - u'_{ab}\right) \end{cases} \tag{13}$$

we have

$$\begin{aligned} &\frac{1}{2}\left(u'_{ab} + u'_{bc}\right)^2 + \frac{1}{2}\left(u'_{bc} - u'_{ab}\right)^2 \\ &\quad - \cos\left(\varphi\right)\left(u'_{ab} + u'_{bc}\right)\left(u'_{bc} - u'_{ab}\right) \\ &\quad = U_m^2 \sin^2\left(\varphi\right). \end{aligned} \tag{14}$$

Simplify (14), it is

$$u'^{\,2}_{ab} + u'^{\,2}_{bc} + \cos\left(\varphi\right) u'^{\,2}_{ab} - \cos\left(\varphi\right) u'^{\,2}_{bc} = U_m^2 \sin^2\left(\varphi\right). \tag{15}$$

Actually, (15) can be written in the standard form of ellipse

$$\frac{u'^{\,2}_{ab}\left(1+\cos\varphi\right)}{U_m^2 \sin^2\left(\varphi\right)} + \frac{u'^{\,2}_{bc}\left(1-\cos\varphi\right)}{U_m^2 \sin^2\left(\varphi\right)} = 1. \tag{16}$$

Under normal conditions, the point (u'_{ab}, u'_{bc}) is on the ellipse and away from (0, 0). According to (16), we have

$$\frac{u'^{\,2}_{ab}\left(1+\cos\varphi\right)}{U_m^2 \sin^2\left(\varphi\right)} + \frac{u'^{\,2}_{bc}\left(1-\cos\varphi\right)}{U_m^2 \sin^2\left(\varphi\right)} = r_d \quad 0 < r_d < 1. \tag{17}$$

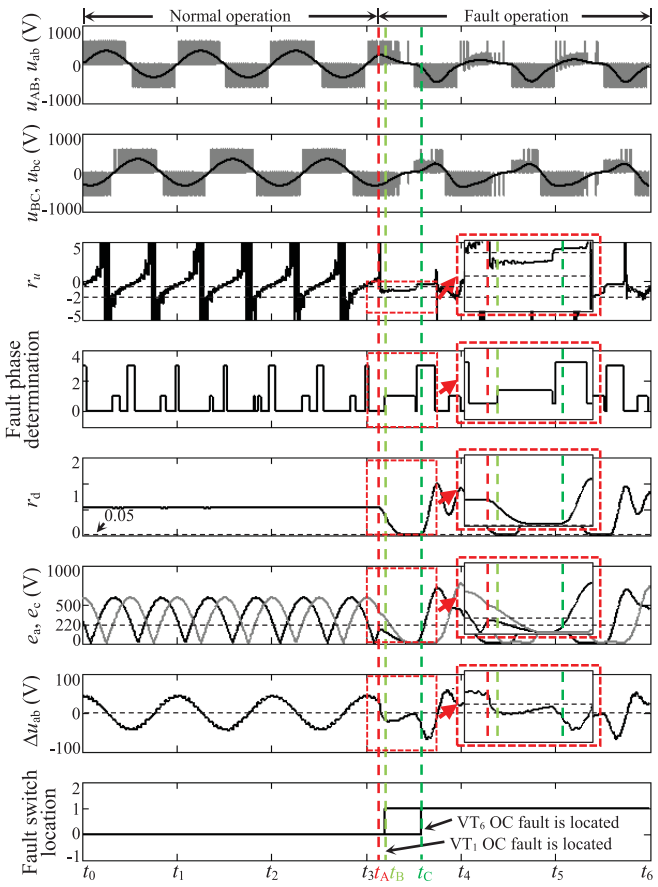

Fig. 9. Diagnosis of VT_1 and VT_6 OC faults.

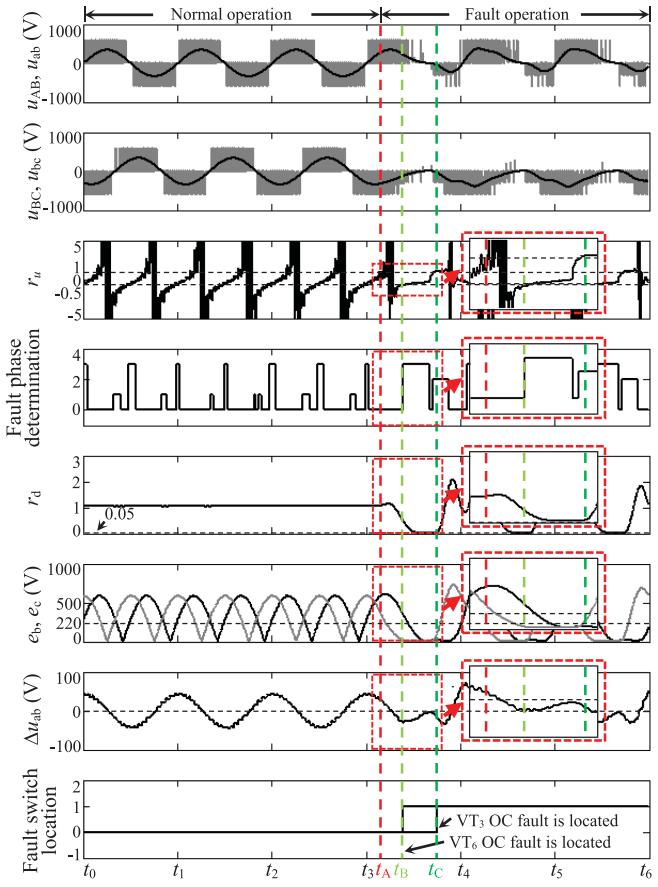

Fig. 10. Diagnosis of VT_3 and VT_6 OC faults.

Equation (17) is a scaled-down ellipse, and the point on the ellipse is closer to (0, 0). The distance from the point (u'_{ab}, u'_{bc}) to (0, 0) can be adjusted proportionally and precisely through adjusting r_d. Therefore, (17) can be used in diagnosis to eliminate the points, which are too close to (0, 0). It can be also written in the form of (7), which is available for (u_{ab}, u_{bc}).

End

In the constraint (7), the parameter α should be less than 1 and is suggested to be a small value. Here, α is 0.05 because it is enough to prevent the errors.

The diagnosis is still unreliable even if the ratio calculation is right. The algorithm in (5) enlarges the fault judgment range while improving the calculation accuracy, thus, it may cause the false detection in some cases. For example, the false detection of a-phase may be triggered under such a situation:

$$\exists e_a \neq 0, \quad u_{bc} = -2u_{ab} + e_a \tag{18}$$

where the error e_a is not within the permissible limits of error. In the situation, the inverter may be actually in a healthy state or a transient state between the normal operation and stable fault operation, but the ratio calculation result erroneously points to the healthy phase. Therefore, we give a constraint to prevent this false detection

$$\begin{cases} \text{a - phase:} & e_a = |2u_{ab}[k] + u_{bc}[k]| < e_{a\_\text{th}} \\ \text{b - phase:} & e_b = |u_{ab}[k] - u_{bc}[k]| < e_{b\_\text{th}} \\ \text{c - phase:} & e_c = |u_{ab}[k] + 2u_{bc}[k]| < e_{c\_\text{th}} \end{cases} \tag{19}$$

where e_{a_th}, e_{b_th}, and e_{c_th} are the thresholds. They should be low positive values, but the noise and interference also need consideration. These thresholds have their maximum values. The constraint will make no sense when the errors e_x (x = a, b, c) are so large that all the points ($u_{ab}[k]$, $u_{bc}[k]$) are contained in the area between the line $u_{bc} = r \cdot u_{ab} + e_x$ and the line $u_{bc} = r \cdot u_{ab} - e_x$. Thus, the maximum values of these thresholds are determined

$$\begin{cases} e_{a\_\max} = |U_m \sin(\varphi)| \sqrt{[5 + 4\cos(\varphi)] / [1 - \cos^2(\varphi)]} \\ e_{b\_\max} = \sqrt{2}\,|U_m \sin(\varphi)| / \sqrt{1 + \cos(\varphi)} \\ e_{c\_\max} = \frac{1}{2}\,|U_m \sin(\varphi)| \sqrt{[5 + 4\cos(\varphi)] / [1 - \cos^2(\varphi)]}. \end{cases} \tag{20}$$

The maximum threshold $e_{a\_\max}$ is proven as follows.

Proof: The tangent on (12) is defined as

$$u_{bc} = -2u_{ab} + e_{a\_\max}. \tag{21}$$

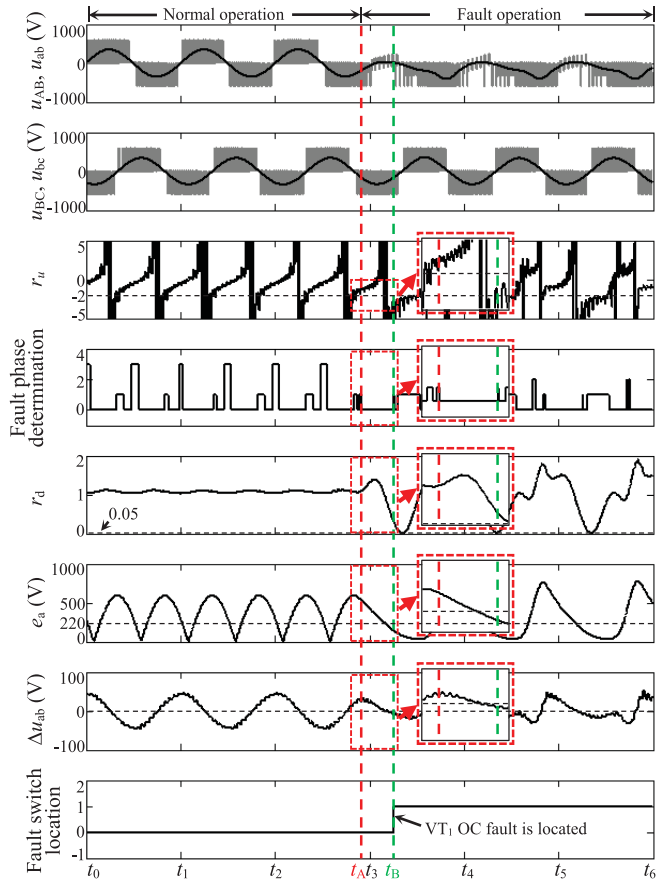

Fig. 11. Diagnosis of VT_1 OC fault under imbalanced load condition.

Then, u_{ab} and u_{bc} are calculated by (12) and (21)

$$\begin{cases} u_{ab} = e_{a\_\max}\left[2+\cos(\varphi)\right]/\left[5+4\cos(\varphi)\right] \\ u_{bc} = e_{a\_\max}\left[1+2\cos(\varphi)\right]/\left[5+4\cos(\varphi)\right]. \end{cases} \tag{22}$$

Thus, $e_{a\_\max}$ can be calculated by plugging (22) into (12)

$$e_{a\_\max} = \left|U_m \sin(\varphi)\right| \sqrt{\left[5+4\cos(\varphi)\right]/\left[1-\cos^2(\varphi)\right]}. \tag{23}$$

Therefore, the maximum tolerable error $e_{a\_\max}$ is proven.

End

Other maximum tolerable errors can be proven in the same way.

Because $\varphi = -2\pi/3$, we have

$$e_{a\_\max} = \sqrt{3}U_m,\ e_{b\_\max} = \sqrt{3}U_m,\ e_{c\_\max} = \frac{\sqrt{3}U_m}{2}. \tag{24}$$

Here, $e_{a\_\text{th}} = e_{b\_\text{th}} = e_{c\_\text{th}} = 220\,\text{V}$.

If the load is a motor, a deviation will exist because of the back electromotive force (EMF). For example, (18) will be

$$u_{bc} = -2u_{ab} + 2E + e_a \tag{25}$$

where E is the back EMF. In this condition, the deviation should be considered when selecting parameters e_{a_th}, e_{b_th}, and e_{c_th}.

C. Fault Switch Location

After the information used for diagnosis is verified to be effective, the fault switch location starts. Generally, line voltage u_{ab} decreases in Z_1 when the OC fault occurs at the upper arm of a-phase. On the contrary, u_{ab} increases in Z_2 when the OC fault occurs at the lower arm of a-phase. This fault feature can be utilized for fault switch location after the fault phase is determined.

Here, voltage difference Δu_{ab} is defined for fault switch location purpose:

$$\Delta u_{ab} = u_{ab}[k] - u_{ab}[k-n+1]. \tag{26}$$

Thus, $\Delta u_{ab} < 0$ when VT_1 OC fault occurs, and $\Delta u_{ab} > 0$ when VT_2 OC fault occurs. Moreover, Δu_{ab} can also be used in fault switch location of both b-phase and c-phase.

It can be seen in Table III that line voltage u_{ab} is equal to line voltage u_{bc} in Z_3 and Z_4. Thus, u_{ab} and u_{bc} decrease in Z_3 when the OC fault occurs at the upper arm of b-phase; u_{ab} and u_{bc} increase in Z_4 when the OC fault occurs at the lower arm of b-phase. As a result, $\Delta u_{ab} < 0$ when VT_3 OC fault occurs, and $\Delta u_{ab} > 0$ when VT_4 OC fault occurs. Similarly, line voltage u_{bc} is equal to line voltage u_{ca} in Z_5 and Z_6. Thus, u_{bc} and u_{ca} decrease in Z_5 when the OC fault occurs at the upper arm of c-phase; u_{bc} and u_{ca} increase in Z_6 when the OC fault occurs at the lower arm of c-phase. However, as observed in Table III, line voltage u_{ab} is inversely proportional to line voltage u_{bc} in Z_5 and Z_6, which means line voltages u_{ab} and u_{ca} also have the opposite trend of change. Therefore, $\Delta u_{ab} > 0$ when VT_5 OC fault occurs, and $\Delta u_{ab} < 0$ when VT_6 OC fault occurs. With the value of Δu_{ab}, all fault switches can be successfully located.

The entire diagnosis process of OC faults in a-phase is shown as an example in Fig. 4. At the beginning, voltages $u_{ab}[k]$, $u_{ab}[k-1]$, …, $u_{ab}[k-n+1]$, $u_{bc}[k]$, $u_{bc}[k-1]$, …, and $u_{bc}[k-n+1]$ are sampled for the calculation of $\mathbf{R}_u$. When $\mathbf{R}_u$ belongs to the range [–2–tan(δ), –2+tan(δ)], the OC fault in phase a is detected. Next, parameter r_d and $|2u_{ab}[k]+u_{bc}[k]|$ are calculated and used for effective diagnosis confirmation. Most of the false alarms under healthy conditions and false diagnosis under faulty conditions can be prevented at this stage. If the diagnosis information is effective, the parameter Δu_{ab} will be calculated. Then, the specific fault switch is located according to Δu_{ab} and the diagnosis at time k is finished. If no fault is detected or the diagnosis information is ineffective, the diagnosis at time k will be ended directly. The diagnosis will go on when the diagnosis process of the previous moment is finished or ended, thus, other OC faults can be identified.

IV. Experimental Results

The proposed fault diagnostic method has been verified on the dSPACE platform, as shown in Fig. 5. The dSPACE platform consists of three parts: hardware, dSPACE real-time system, and software. The hardware part mainly includes a dc power, an inverter, and adjustable load. dSPACE real-time system includes a DS1007 Processor Board, a DS2002 High Precision A/D Board, and a DS4004 High Speed I/O Board. The software part contains

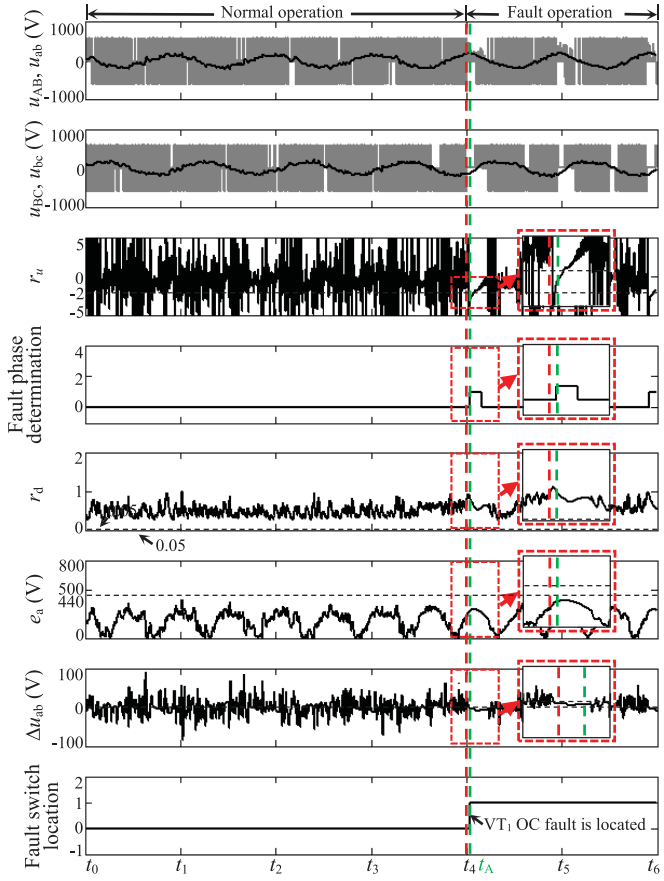

Fig. 12. Diagnosis of VT_1 OC fault under motor load condition: rotor speed = 600 r/min.

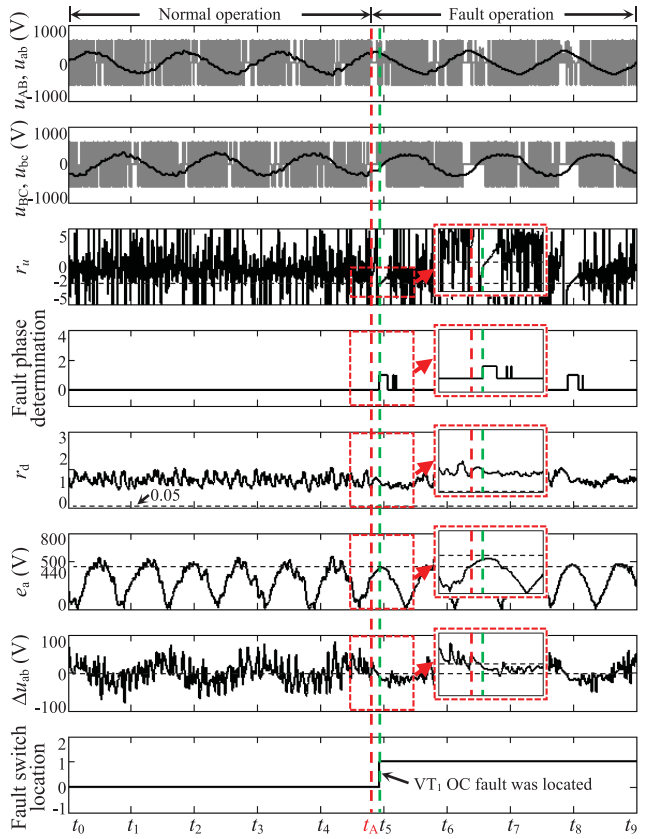

Fig. 13. Diagnosis of VT_1 OC fault under motor load condition: rotor speed = 1200 r/min.

the Simulink Platform, the Real-Time Workshop, the Real-Time Interface, and the Control Desk. The original diagnosis model is built in the Simulink Platform, and is converted into C codes, which can be used in DSP system by the real-time workshop. The C codes runs in the dSPACE real-time system after loaded into the real-time interface. The variables of the diagnosis model are accessible in the control desk. They can be exported and saved in the computer. Thus, it is convenient to monitor the operation of the system online and offline.

The key parameters of the prototype are given in Table IV. Considering the noise and interference, the sampling queue length n is increased to six to ensure the robustness of the method. But it is not recommended to choose a large value, because it will only bring more computational burden to the algorithm.

In the experiment, OC fault is simulated by blocking the control signal of the switch, and double faults are simulated by blocking the control signals simultaneously. Line voltages u_{ab} and u_{bc} are collected by the inherent sensors of the inverter. To have a clear view of the waveforms, voltages $u_{\rm AB}$ and $u_{\rm BC}$ are also monitored. But they are not used in the diagnosis system. The fault phase determination signal value "1" represents a-phase, "2" b-phase, and "3" c-phase. Six fault switch location signals are used to represent the diagnosis results. The signal output is "0" under healthy condition, and "1" after the fault switch is located.

A. SSOC and DSOC Faults Diagnosis

The waveforms of VT_1 OC fault is shown in Fig. 6. Before the VT_1 OC fault occurs, the fault phase determination signal appears periodically because the situation in (18) appears. But these false phase determinations are all avoided by the effective diagnosis confirmation and are not used for the future diagnosis. As the difference between two sinusoidal waves, Δu_{ab} also varies regularly. The VT_1 OC fault occurs at t_B. After a short period, failure in a-phase is detected again, and the information is verified to be effective this time. The signal Δu_{ab} suddenly decreased to a negative value. Then, VT_1 OC fault is located at t_C. The entire process from fault occurrence to fault location takes 0.0034 s.

Fig. 7 shows the diagnosis of DSOC faults in phase a. Because the time zones of OC faults are different from each other, the OC faults are located sequentially. The DSOC faults are simulated at t_A, and the failure in a-phase is quickly detected at t_B. At the same time, Δu_{ab} is lower than zero, and VT_1 OC fault is located. VT_2 OC fault is located until Δu_{ab} increases to higher than zero. The entire process takes approximately half of the period. Fig. 8 presents the DSOC faults in phases a and b. VT_1 OC fault is rapidly detected and located after faults are simulated. Because the time zone of VT_3 OC fault follows that of VT_1 OC fault, VT_3 OC fault is located after a relatively long period. The entire process also takes approximately half of the period. Fig. 9 presents the DSOC faults in phases a and c. The time zone of

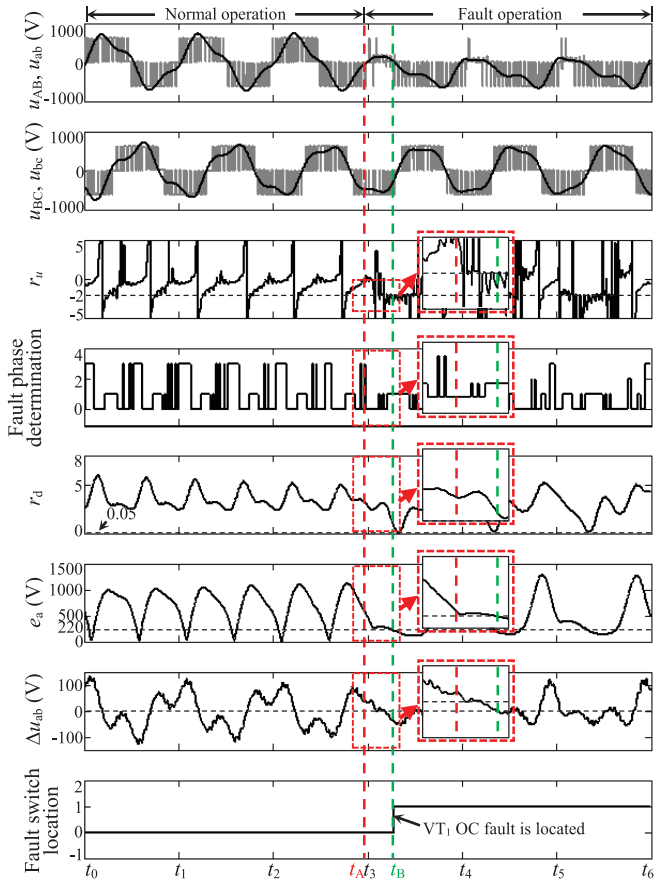

Fig. 14. Diagnosis of VT_1 OC fault under no-load condition.

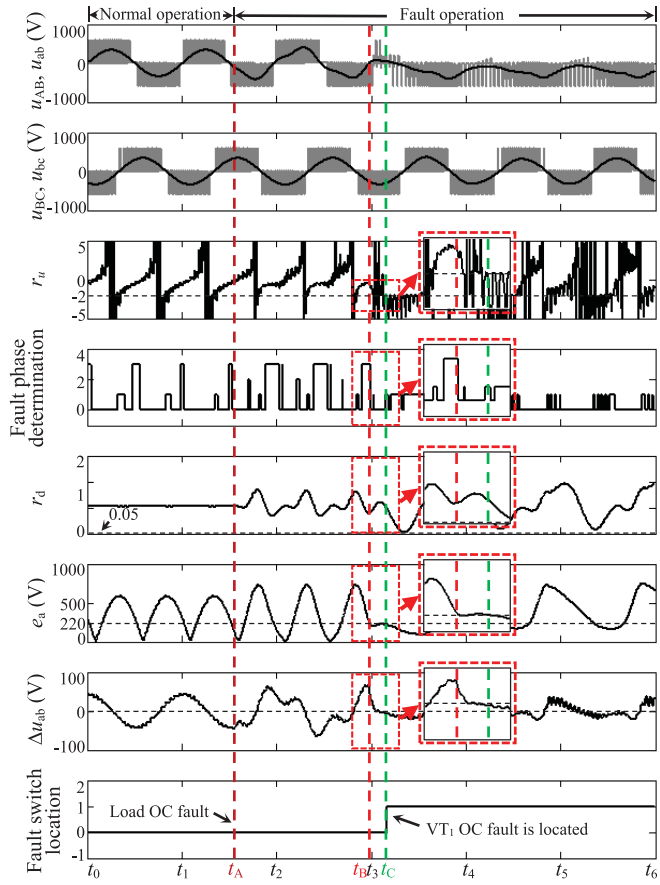

Fig. 15. Diagnosis of VT_1 OC fault under load OC fault condition.

VT_6 OC fault is behind that of VT_1 OC fault but not far from it. Consequently, VT_1 is located at t_B, and VT_6 is quickly located at t_C. The entire process takes 0.0092 s, less than half of the period. Fig. 10 shows the DSOC faults in phases b and c. The time zone of VT_3 OC fault is behind that of VT_6 OC fault but also not far from it. VT_3 OC fault is located quickly after VT_6 OC fault is located. However, the time consumption of the entire process depends on the fault finally located. The entire process takes approximately half of the period.

B. Robustness to Load Conditions and the Load OC Fault

The robustness of the proposed method to different load conditions and the load OC fault is verified by the following experimental results. Fig. 11 presents the diagnosis of VT_1 OC fault under imbalanced load condition. A resistor of 20 Ω is connected in series in a-phase. Consequently, phase currents i_a decreases slightly, i_b increases, and i_c decreases. The imbalance also has a small effect on the voltage u_{AB} near t_3, compared with the voltage in Fig. 6. However, it does not have any obvious influence on the diagnosis or the result. VT_1 OC fault is simulated at t_A and successfully located at t_B. Fig. 6 also shows the influence of load change on the proposed method. The load changes from 3 to 9 kW at t_A, but does not cause any false alarms. VT_1 OC fault occurs at t_B and is successfully located at t_C. The proposed method is also robust to no-load conditions in some cases. Figs. 12 and 13 show the diagnosis when the load is a direct torque controlled motor. Voltages are proportionately adjusted in the figure for better visual effect. During the diagnosis, the values of parameters e_{a_th}, e_{b_th}, and e_{c_th} are increased considering the effect of back EMF. But the back EMF does not have a critical influence on the proposed method. In Fig. 12, the fault is located as soon as it appears. In Fig. 13, the fault is set at t_A, and quickly located near t_5. The entire process is less than 1/10 cycle. Fig. 14 shows the diagnosis when the load is disconnected with the inverter and the open-loop control is adopted. It can be seen that the voltage waveforms are already unsatisfactory before the fault occurs and the false alarms also appear more frequently. But this influence does not change the diagnosis result. The false diagnosis is avoided and the VT_1 OC fault is accurately located at t_B.

Except these load conditions, the impact of another possible OC fault that occurs at the output side is simulated as well. Fig. 15 presents the influence of load OC fault of a-phase on the proposed method. A contactor is connected in series with the load in a-phase to simulate the load OC fault, and the fault occurs at t_A. Although the fault has an influence on the voltages and diagnosis parameters, it did not cause any false alarms. VT_1 OC fault occurs at t_B and is accurately located at t_C. This diagnosis process takes 0.0048 s. However, the proposed method is not applicable when two phases are shorted at the output side.

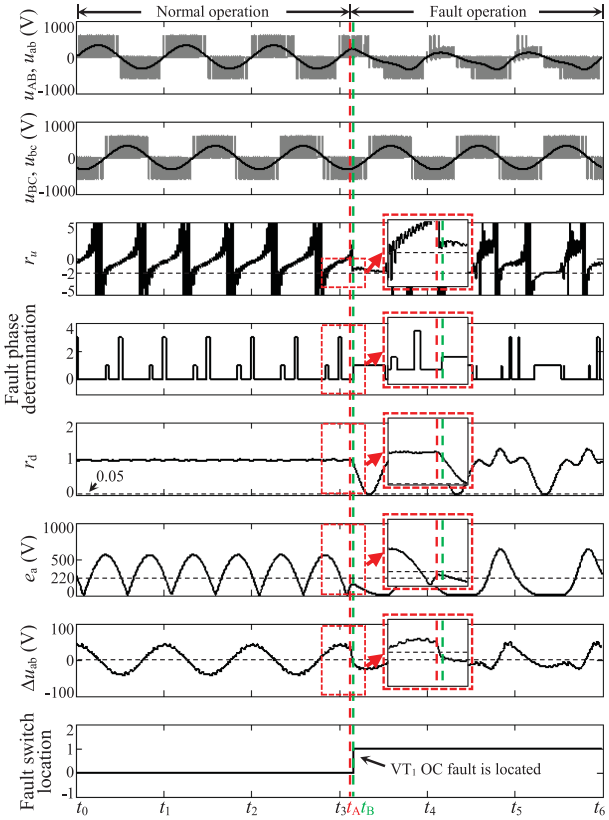

Fig. 16. Diagnosis for an SVPWM-based inverter.

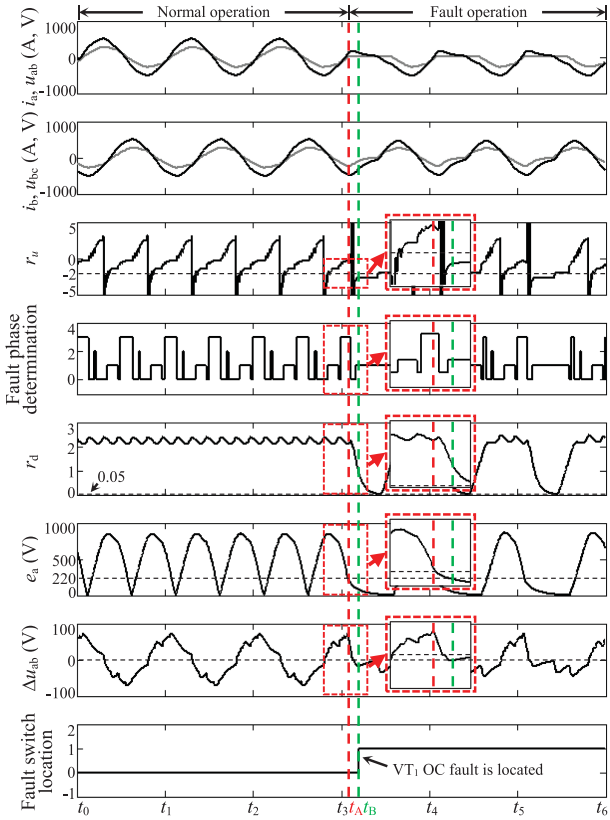

Fig. 17. Diagnosis for a hysteresis current PWM-based inverter.

C. Robustness to Different Control Strategies

The robustness of the proposed method to different control strategies is verified by applying the method to an space vector pulse width modulation (SVPWM)-based inverter and a hysteresis current pulsewitdth modulation (PWM)-based inverter. It should be noted that extra filters or algorithms are needed to convert $u_{\rm AB}$ and $u_{\rm BC}$ into u_{ab} and u_{bc} if the inverter system does not have the *LC* components at the output side. Fig. 16 shows the diagnosis for VT$_1$ OC fault of an SVPWM-based inverter. As observed, the fault occurs at t_A and was quickly located at t_B. The entire diagnosis process takes only 0.001 s. The diagnosis result is not affected because the voltage magnitude of each control state remains unchanged. Fig. 17 shows the diagnosis for VT$_1$ OC fault of a hysteresis current PWM-based inverter. The currents i_a and i_b are amplified for better visual effect. It can be seen that the control strategy has influence on the diagnosis parameters and the distorted voltages. A false faulty phase determination signal is observed frequently, and the amplitudes of other diagnosis parameters also increase. Both u_{ab} and u_{bc} are distorted after VT$_1$ OC fault occurs at t_A. However, the amplitude increase of r_d, e_a, and Δu_{ab} will not cause the false diagnosis. The diagnosis method remains accurate and VT$_1$ OC fault is successfully located at t_B. The entire diagnosis process takes 0.0045 s.

D. Robustness to Output Filter Components and Carrier Frequency

The filter parameters are changed in the normal range to verify the performance of the proposed method. Fig. 18 shows the diagnosis of VT$_1$ OC fault under the higher harmonics condition, and Fig. 19 shows the diagnosis under the lower harmonics condition. When the harmonics increase, the fault phase determination has a better performance and the parameter r_d is more stable. When the harmonics decrease, the parameters r_u and Δu_{ab} are smoother. The error e_a is not significantly affected. No matter how the filter components change, the VT$_1$ OC faults are all accurately located in the end.

Fig. 20 shows the diagnosis of VT$_1$ OC fault when carrier frequency increases to 6 kHz. The waveforms of r_u and Δu_{ab} became smoother. In the other hand, the fault phase determination signal appears more frequently. VT$_1$ OC fault occurs at t_3, and is located at t_A rapidly. The entire diagnosis process takes 0.0036 s.

E. Influence of Fault Occurrence Time

The fault occurrence time has influence on the diagnosis time consumption. For SSOC faults, the OC fault can be located immediately if the fault occurs before the time zone, such as the diagnosis in Fig. 8, and the time consumption is around 1/20 of the period. In the worst cases, the diagnosis time consumption is about half of the period. A fault diagnosis time distribution over a fundamental period is summarized as an example in Fig. 21. In the figure, the fundamental period is 0.02 s. The yellow part represents the percentage of the actual diagnosis time from the fault appearance to fault location. The lowest percentage is 5%, 0.001 s. The highest one reaches to 40%, about 0.008 s. In most situations, the percentage is 27%, i.e., 0.0054 s. In addition, there

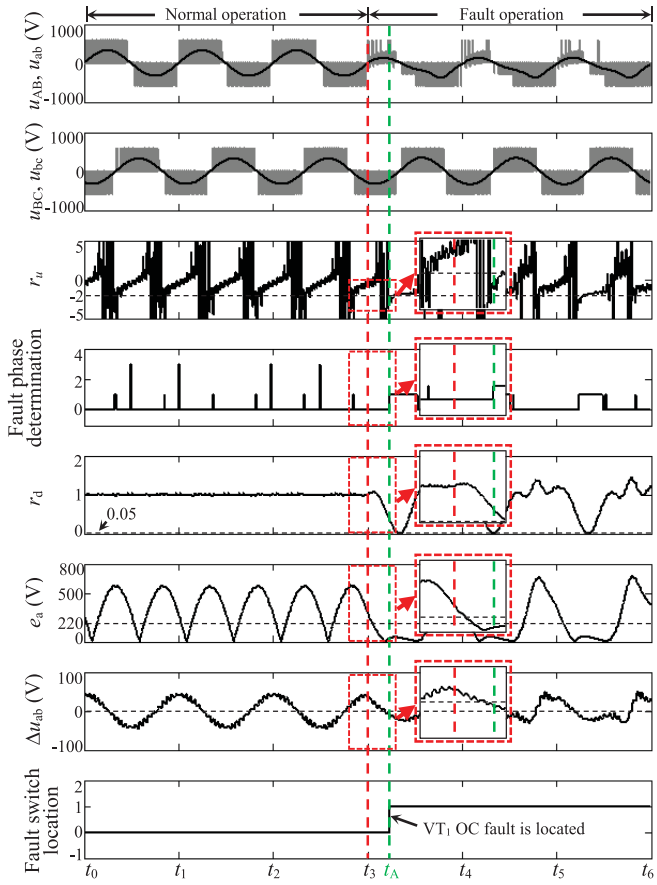

Fig. 18. Diagnosis of VT_1 OC fault when $L_a = L_b = L_c = 4$ mH and $C_5 = C_6 = C_7 = 60$ μF.

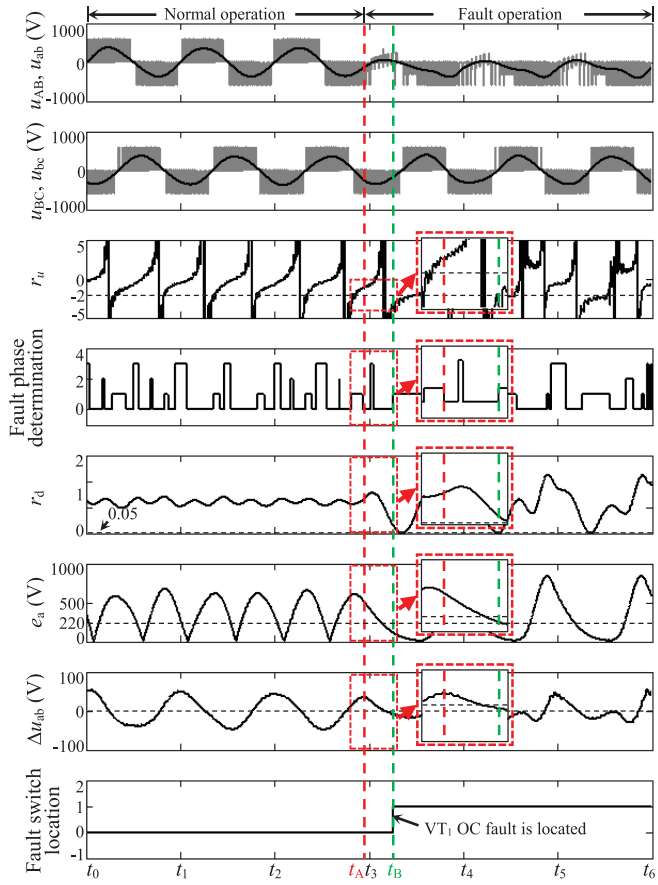

Fig. 19. Diagnosis of VT_1 OC fault when $L_a = L_b = L_c = 5$ mH and $C_5 = C_6 = C_7 = 150$ μF.

is a situation should be noted. When VT_1 OC fault is simulated near the region where voltage u_{AB} is nonpositive, the system still works in a "healthy condition" for a period of time. In this condition, the waveforms are normal because of the antiparallel diode, and this can last up to half of the period. The fault is hardly detected without extra devices. However, it also has little impact on the system for the time being. Therefore, this phenomenon exists but is usually ignored in most of the existing literatures. In this article, the healthy operation time is also recorded in green in Fig. 21. This may bring the more comprehensive understanding of the influence of fault occurrence time.

Because the proposed method needs two time zones for DSOC faults diagnosis, the diagnosis time consumption depends on the fault occurrence time and the second time zone, and the average diagnosis time consumption is usually longer than that of SSOC faults. The longest diagnosis time consumption is one period. The diagnosis process is shorter if the faults occur before the two time zones and the two time zones have an overlapped part. For example, the diagnosis in Fig. 6, which only takes 0.0092 s, less than half of the period.

V. Comparison With Existing Diagnosis Methods

Table V shows the comparison of the proposed method with other fault diagnosis methods presented in recent years.

Each row of Table V is divided by the longest diagnosis time consumption. Because not all the methods are able to locate DSOC faults, the longest diagnosis time consumption only refers to the situation of SSOC faults. The first row lists the methods which can finish the diagnosis in half of the period, and the proposed method is also included here. However, there are still more than half of the methods, which require one or even two fundamental periods for diagnosis, and these methods are listed in the second row.

Each column of Table V is divided by the number of information sources and the utilization of extra devices. The methods in the second column combine various diagnosis variables, such as three-phase currents, dc-link voltage, angular velocity, control signals, and electromagnetic signatures collected by an extra near-field antenna. It is generally thought that more information sources mean higher reliability and more accurate diagnosis results. However, this may be the opposite in some situations. Actually, the accurate fault diagnosis is based on the accurate information, and any false information may lead to the overlook or the false result of the diagnosis. Therefore, undue information sources may even increase the error rate of the diagnosis. For example, assuming that all resources are properly used, and the failure rate of each information source is equal. If the failure rate is 1% (which should normally be much lower, here it is just used for demonstration), then, the rate of overlook or false diagnosis

TABLE V
COMPARISON OF THE PROPOSED METHOD WITH EXISTING DIAGNOSIS METHODS

Fault diagnosis methods	(Two information sources) AND (No extra device is required)	(More than two information sources) OR (Other device is required)
The longest diagnosis time is less than half of the period	Voltage-based method: The proposed method*, [25]*, [49]	Current-based methods: [10]*, [12]*, [15]* Voltage-based method: [50]* Multi-source information based methods: [17]*, [21]*, [22], [23], [24], [28], [32], [33]*, [34], [36]*, [40], [42]*
The longest diagnosis time is more than half of the period	Current-based method: [11]	Current-based methods: [8]*, [9], [16]*, [18]*, [51]*, [52]*, [53]; Voltage-based method: [20]; Multi-source information based methods: [19], [29]*, [30]*, [31]*, [35], [37], [38]*, [39], [41]*, [54]
Unknown diagnosis time	None	Voltage-based methods: [26], [27]

Note: $*$ means the method is able to locate DSOC faults or a part of DSOC faults.

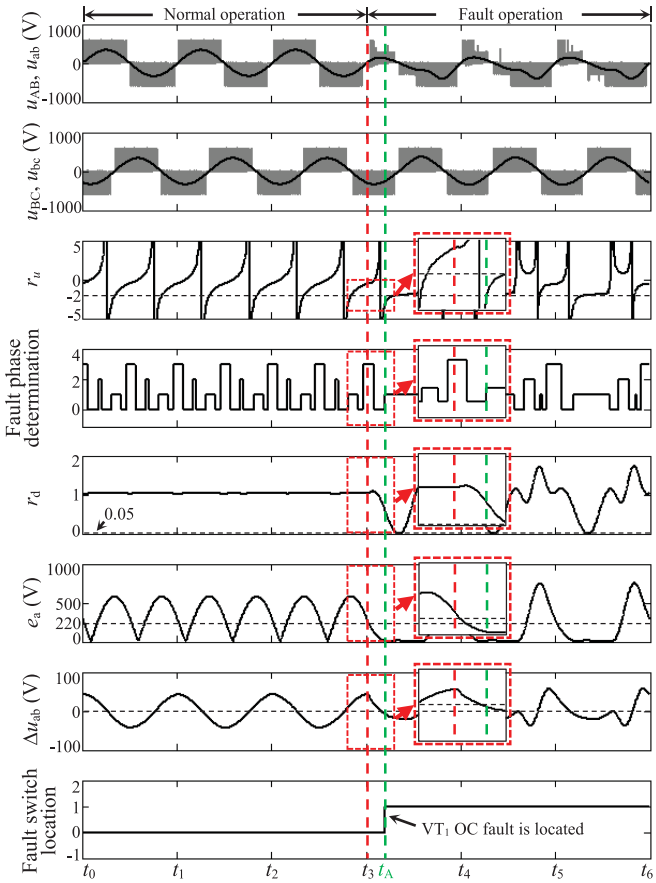

Fig. 20. Diagnosis of VT_1 OC fault when the carrier frequency is 6 kHz.

using two information sources is

$$(1 - 0.99 \times 0.99) \times 100\% = 1.99\%;$$

and the one using three information sources is

$$(1 - 0.99 \times 0.99 \times 0.99) \times 100\% = 2.97\%.$$

It can be seen that the rate in the second case is much higher than that in the first case. Therefore, more information sources do not necessarily mean higher diagnostic reliability, they may even increase the error rate. Moreover, the measurement accuracy of the various information may be inconsistent in some conditions. The

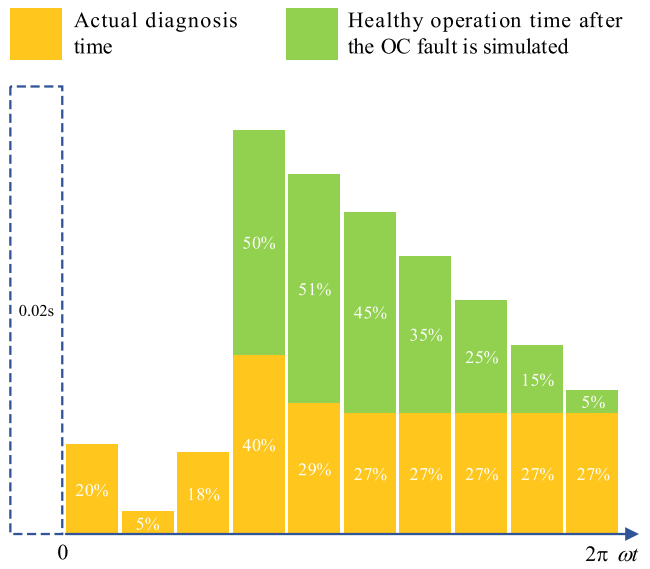

Fig. 21. VT_1 OC fault diagnosis time distribution over a fundamental period.

accuracy of the diagnosis ultimately depends on the information with the lowest accuracy. Therefore, these methods may have the disadvantages of resources wasting and the decline in diagnostic accuracy. Compared with these methods, the proposed method uses only two information sources for diagnosis purpose to avoid the problems. At the same time, the diagnosis speed and accuracy are also guaranteed.

The proposed method is able to quickly locate DSOC faults, which is superior to the voltage-envelop-based method in [49]. Compared with the Bayesian-network-based method in [25], there is no complex network structure design or complicated training in the proposed method. The proposed method has less calculation and is more convenient to apply to other systems. Moreover, the proposed method is robust to different load conditions and immune to certain load OC faults. It is more suitable for the application that requires high reliability.

VI. CONCLUSION

In this article, a new OC faults diagnostic method is proposed for voltage-source inverters. Two line voltages are used as diagnosis variables for reliability and economy. Possible magnitudes

of these line voltages are characterized in detail both for the healthy and faulty operations. The fault phase can be determined by the magnitude ratio of two line voltages, and the fault switch can be located by the voltage difference. Effective diagnosis confirmation is also adopted in the method to prevent false diagnosis. Both SSOC and DSOC faults can be accurately identified by the proposed method. The fastest diagnosis processes of SSOC and DSOC faults can be finished in 1/20 of the fundamental period and half of the period, respectively. In comparison, nearly half of the existing methods require one or more periods to finish the SSOC diagnosis. The proposed method is robust to different load conditions, filter components, and carrier frequencies. It is also verified to be immune to certain load OC faults, which may lead to the false diagnosis of the existing methods and have not been discussed in current literatures. With a few adjustments, this diagnostic method can be applied to SVPWM-based and hysteresis current PWM-based inverters. Moreover, neither the control signals nor extra devices are needed for implementation. Thus, the proposed method can be applied to both existing and newly built inverters.

REFERENCES

[1] B. Lu and S. K. Sharma, "A literature review of IGBT fault diagnostic and protection methods for power inverters," *IEEE Trans. Ind. Appl.*, vol. 45, no. 5, pp. 1770–1777, Jul. 2009.

[2] R. R. Errabelli and P. Mutschler, "Fault-tolerant voltage source inverter for permanent magnet drives," *IEEE Trans. Power Electron.*, vol. 27, no. 2, pp. 500–508, Apr. 2011.

[3] U. Choi, F. Blaabjerg, and K. Lee, "Reliability improvement of a T-type three-level inverter with fault-tolerant control strategy," *IEEE Trans. Power Electron.*, vol. 30, no. 5, pp. 2660–2673, May 2014.

[4] U. Choi, J. Lee, F. Blaabjerg, and K. Lee, "Open-circuit fault diagnosis and fault-tolerant control for a grid-connected NPC inverter," *IEEE Trans. Power Electron.*, vol. 31, no. 10, pp. 7234–7247, Dec. 2015.

[5] D. Zhou, Y. Li, J. Zhao, F. Wu, and H. Luo, "An embedded closed-loop fault-tolerant control scheme for nonredundant VSI-fed induction motor drives," *IEEE Trans. Power Electron.*, vol. 32, no. 5, pp. 3731–3740, Jun. 2016.

[6] A. Mohammadpour, S. Sadeghi, and L. Parsa, "A generalized fault-tolerant control strategy for five-phase PM motor drives considering star, pentagon, and pentacle connections of stator windings," *IEEE Trans. Ind. Electron.*, vol. 61, no. 1, pp. 63–75, Feb. 2013.

[7] N. K. Nguyen, F. Meinguet, E. Semail, and X. Kestelyn, "Fault-tolerant operation of an open-end winding five-phase PMSM drive with short-circuit inverter fault," *IEEE Trans. Ind. Electron.*, vol. 63, no. 1, pp. 595–605, Jan. 2015.

[8] U. Choi, J. Lee, F. Blaabjerg, and K. Lee, "Open-circuit fault diagnosis and fault-tolerant control for a grid-connected NPC inverter," *IEEE Trans. Power Electron.*, vol. 31, no. 10, pp. 7234–7247, Dec. 2015.

[9] U. Choi, H. Jeong, K. Lee, and F. Blaabjerg, "Method for detecting an open-switch fault in a grid-connected NPC inverter system," *IEEE Trans. Power Electron.*, vol. 27, no. 6, pp. 2726–2739, Dec. 2011.

[10] W. Sleszynski, J. Nieznanski, and A. Cichowski, "Open-transistor fault diagnostics in voltage-source inverters by analyzing the load currents," *IEEE Trans. Ind. Electron.*, vol. 56, no. 11, pp. 4681–4688, Jun. 2009.

[11] F. Zidani, D. Diallo, M. E. H. Benbouzid, and R. Nait-Said, "A fuzzy-based approach for the diagnosis of fault modes in a voltage-fed PWM inverter induction motor drive," *IEEE Trans. Ind. Electron.*, vol. 55, no. 2, pp. 586–593, Jan. 2008.

[12] N. M. A. Freire, J. O. Estima, and A. J. M. Cardoso, "Open-circuit fault diagnosis in PMSG drives for wind turbine applications," *IEEE Trans. Ind. Electron.*, vol. 60, no. 9, pp. 3957–3967, Jul. 2012.

[13] H. Chen and S. Lu, "Fault diagnosis digital method for power transistors in power converters of switched reluctance motors," *IEEE Trans. Ind. Electron.*, vol. 60, no. 2, pp. 749–763, Jul. 2012.

[14] B. Gou, X. Ge, and Y. Liu, "Load-current-based current sensor fault diagnosis and tolerant control scheme for traction inverters," *Electron. Lett.*, vol. 52, no. 20, pp. 1717–1719, Sep. 2016.

[15] J. O. Estima and A. J. M. Cardoso, "A new approach for real-time multiple open-circuit fault diagnosis in voltage-source inverters," *IEEE Trans. Ind. Appl.*, vol. 47, no. 6, pp. 2487–2494, Sep. 2011.

[16] J. Choi, S. Kim, D. S. Yoo, and K. Kim, "A diagnostic method of simultaneous open-switch faults in inverter-fed linear induction motor drive for reliability enhancement," *IEEE Trans. Ind. Electron.*, vol. 62, no. 7, pp. 4065–4077, Dec. 2014.

[17] I. Jlassi, J. O. Estima, S. K. E. Khil, N. M. Bellaaj, and A. J. M. Cardoso, "A robust observer-based method for IGBTs and current sensors fault diagnosis in voltage-source inverters of PMSM drives," *IEEE Trans. Ind. Appl.*, vol. 53, no. 3, pp. 2894–2905, Oct. 2016.

[18] J. Zhang, J. Zhao, and D. Zhou, "High-performance fault diagnosis in PWM voltage-source inverters for vector-controlled induction motor drives," *IEEE Trans. Power Electron.*, vol. 29, no. 11, pp. 6087–6099, Jan. 2014.

[19] S. Karimi, P. Pourse, and S. Saadate, "Fast power switch failure detection for fault tolerant voltage source inverters using FPGA," *IET Power Electron.*, vol. 2, no. 4, pp. 346–354, Jul. 2009.

[20] R. L. de A. Ribeiro, C. B. Jacobina, E. R. C. da Silva, and A. M. N. Lima, "Fault detection of open-switch damage in voltage-fed PWM motor drive systems," *IEEE Trans. Power Electron.*, vol. 18, no. 2, pp. 587–593, Mar. 2003.

[21] Q. T. An, L. Sun, and L. Z. Sun, "Hardware-circuit-based diagnostic method for open-switch faults in inverters," *Electron. Lett.*, vol. 49, no. 17, pp. 1089–1091, Aug. 2013.

[22] Q. T. An, L. Z. Sun, and L. Sun, "Low-cost diagnostic method for open-switch faults in inverters," *Electron. Lett.*, vol. 46, no. 14, pp. 1021–1022, Jul. 2010.

[23] Q. T. An, L. Z. Sun, K. Zhao, and L. Sun, "Switching function model-based fast-diagnostic method of open-switch faults in inverters without sensors," *IEEE Trans. Power Electron.*, vol. 26, no. 1, pp. 119–126, Jun. 2010.

[24] C. Choi and W. Lee, "Design and evaluation of voltage measurement-based sectoral diagnostic method for inverter open switch faults of permanent magnet synchronous motor drives," *IET Elect. Power Appl.*, vol. 6, no. 8, pp. 526–532, Aug. 2012.

[25] T. Wang, H. Xu, J. Han, E. Elbouchikhi, and M. Benbouzid, "Cascaded H-bridge multilevel inverter system fault diagnosis using a PCA and multi-class relevance vector machine approach," *IEEE Trans. Power Electron.*, vol. 30, no. 12, pp. 7006–7018, Dec. 2015.

[26] B. Cai, Y. Zhao, H. Liu, and M. Xie, "A data-driven fault diagnostic methodology in three-phase inverters for PMSM drive systems," *IEEE Trans. Power Electron.*, vol. 32, no. 7, pp. 5590–5600, Sep. 2016.

[27] S. Khomfoi and L. M. Tolbert, "Fault diagnosis and reconfiguration for multilevel inverter drive using AI-based techniques," *IEEE Trans. Ind. Electron.*, vol. 54, no. 6, pp. 2954–2968, Oct. 2007.

[28] S. Khomfoi and L. M. Tolbert, "Fault diagnostic system for a multilevel inverter using a neural network," *IEEE Trans. Power Electron.*, vol. 22, no. 3, pp. 1062–1069, May 2007.

[29] J. He, N. A. O. Demerdash, and N. Weise, "A fast on-line diagnostic method for open-circuit switch faults in SiC-MOSFET-based T-type multi-level inverters," *IEEE Trans. Industry Appl.*, vol. 53, no. 3, pp. 2948–2958, Jan. 2017.

[30] F. Meinguet, P. Sandulescu, X. Kestelyn, and E. Semail, "A method for fault detection and isolation based on the processing of multiple diagnostic indices: Application to inverter faults in AC drives," *IEEE Trans. Veh. Technol.*, vol. 62, no. 3, pp. 995–1009, Dec. 2012.

[31] F. Wu and J. Zhao, "A real-time multiple open-circuit fault diagnostic method in voltage-source-inverter fed vector controlled drives," *IEEE Trans. Power Electron.*, vol. 31, no. 2, pp. 1425–1437, Apr. 2015.

[32] F. Wu, J. Zhao, and Y. Liu, "Symmetry-analysis-based diagnostic method with correlation coefficients for open-circuit fault in inverter," *Electron. Lett.*, vol. 51, no. 21, pp. 1688–1690, Oct. 2015.

[33] S. Jung, J. Park, H. Kim, K. Cho, and M. Youn, "An MRAS-based diagnosis of open-circuit fault in PWM voltage-source inverters for PM synchronous motor drive systems," *IEEE Trans. Power Electron.*, vol. 28, no. 5, pp. 2514–2526, Aug. 2012.

[34] Q. T. An, L. Sun, and L. Z. Sun, "Current residual vector-based open-switch fault diagnosis of inverters in PMSM drive systems," *IEEE Trans. Power Electron.*, vol. 30, no. 5, pp. 2814–2827, Sep. 2014.

[35] B. Li, S. Shi, and B. Wang, "Fault diagnosis and tolerant control of single IGBT open-circuit failure in modular multilevel converters," *IEEE Trans. Power Electron.*, vol. 31, no. 4, pp. 3165–3176, Jul. 2015.
[36] U. Choi, K. Lee, and F. Blaabjerg, "Diagnosis and tolerant strategy of an open-switch fault for T-type three-level inverter systems," *IEEE Trans. Ind. Appl.*, vol. 50, no. 1, pp. 495–508, Jun. 2013.
[37] M. B. Abadi, A. M. S. Mendes, and S. M. A. Cruz, "Method to diagnose open-circuit faults in active power switches and clamp diodes of three-level neutral-point clamped inverters," *IET Elect. Power Appl.*, vol. 10, no. 7, pp. 623–632, Jul. 2016.
[38] D. R. Espinoza-Trejo, D. U. Campos-Delgado, E. Barcenas, and F. J. Martinez-Lopez, "Robust fault diagnosis scheme for open-circuit faults in voltage source inverters feeding induction motors by using non-linear proportional-integral observers," *IET Power Electron.*, vol. 5, no. 7, pp. 1204–1216, Oct. 2012.
[39] J. Lamb and B. Mirafzal, "Open-circuit IGBT fault detection and location isolation for cascaded multilevel converters," *IEEE Trans. Ind. Electron.*, vol. 64, no. 6, pp. 4846–4856, Jun. 2017.
[40] K. O. Mtepele, D. U. Campos-Delgado, A. A. Valdez-Fernández, and J. A. PecinaSánchez, "Model-based strategy for open-circuit faults diagnosis in n-level CHB multilevel converters," *IET Power Electron.*, vol. 12, no. 4, pp. 648–655, Feb. 2019.
[41] J. Hang, J. Zhang, M. Cheng, and S. Ding, "Detection and discrimination of open-phase fault in permanent magnet synchronous motor drive system," *IEEE Trans. Power Electron.*, vol. 31, no. 7, pp. 4697–4709, Sep. 2015.
[42] M. A. Masrur, Z. Chen, and Y. Murphey, "Intelligent diagnosis of open and short circuit faults in electric drive inverters for real-time applications," *IET Power Electron.*, vol. 3, no. 2, pp. 279–291, Feb. 2010.
[43] N. M. A. Freire, J. O. Estima, and A. J. M. Cardoso, "A voltage-based approach without extra hardware for open-circuit fault diagnosis in closed-loop PWM AC regenerative drives," *IEEE Trans. Ind. Electron.*, vol. 61, no. 9, pp. 4960–4970, Aug. 2013.
[44] H. Yan, Y. Xu, J. Zou, Y. Fang, and F. Cai, "A novel open-circuit fault diagnosis method for voltage source inverters with a single current sensor," *IEEE Trans. Power Electron.*, vol. 33, no. 10, pp. 8775–8786, Oct. 2018.
[45] J. O. Estima and A. J. M. Cardoso, "A new algorithm for real-time multiple open-circuit fault diagnosis in voltage-fed PWM motor drives by the reference current errors," *IEEE Trans. Ind. Electron.*, vol. 60, no. 8, pp. 3496–3505, Aug. 2013.
[46] P. Lezana, R. Aguilera, and J. Rodríguez, "Fault detection on multicell converter based on output voltage frequency analysis," *IEEE Trans. Ind. Electron.*, vol. 56, no. 6, pp. 2275–2283, Jun. 2009.
[47] Y. Yu, Y. Zhao, B. Wang, X. Huang, and D. Xu, "Current sensor fault diagnosis and tolerant control for VSI-based induction motor drives," *IEEE Trans. Power Electron.*, vol. 33, no. 5, pp. 4238–4248, Jun. 2017.
[48] T. A. Najafabadi, F. R. Salmasi, and P. Jabehdar-Maralani, "Detection and isolation of speed-, DC-link voltage-, and current-sensor faults based on an adaptive observer in induction-motor drives," *IEEE Trans. Ind. Electron.*, vol. 58, no. 5, pp. 1662–1672, Jul. 2010.
[49] C. Gaohua, C. Shu, and X. Chaoqun, "A non-intrusive diagnostic technique for open-circuited faults of inverters," *Proc. CSEE*, vol. 37, no. 13, pp. 3854–3862, Jul. 2017.
[50] H. Jun, Z. Jianzhong, C. Ming, D. Shichuan, and L. Guoli, "Fault diagnosis of open-circuit faults in converters of direct-driven permanent magnet wind power generation systems based on line voltage errors," *Proc. CSEE*, vol. 37, no. 10, pp. 2933–2943, May 2017.
[51] Z. Huang, Z. Wang, and H. Zhang, "Multiple open-circuit fault diagnosis based on multistate data processing and subsection fluctuation analysis for photovoltaic inverter," *IEEE Trans. Instrum. Meas.*, vol. 67, no. 3, pp. 516–526, Mar. 2018.
[52] Z. Huang, Z. Wang, and H. Zhang, "A diagnosis algorithm for multiple open-circuited faults of microgrid inverters based on main fault component analysis," *IEEE Trans. Energy Convers.*, vol. 33, no. 3, pp. 925–937, Sep. 2018.
[53] Z. Wang, Z. Huang, C. Song, and H. Zhang, "Multiscale adaptive fault diagnosis based on signal symmetry reconstitution preprocessing for microgrid inverter under changing load condition," *IEEE Trans. Smart Grid*, vol. 9, no. 2, pp. 797–806, Mar. 2018.
[54] M. Dong, H. Dong, L. Wang, J. Yang, L. Li, and Y. Wang, "A simple open-circuit detection strategy for a single-phase grid-connected PV inverter fed from power optimizers," *IEEE Trans. Power Electron.*, vol. 33, no. 4, pp. 2798–2802, Apr. 2018.

Xun Wu was born in Xinhua, China, in 1993. He received the B.E. degree in electrical engineering and the Ph.D. degree in traffic information engineering and control from Central South University, Changsha, China, in 2015 and 2019, respectively.

From 2018 to 2019, he was a Visiting Scholar with California PATH, University of California Berkeley, Berkeley, CA, USA. His research interests include control techniques and fault diagnosis of power electronic converters, life-prediction of capacitors, and safety analysis.

Chun-Yang Chen was born in Nanling, China, in 1962. He received the B.E. degree in electric locomotive from Southwest Jiaotong University, Chengdu, China, the master's degree from Hunan University, Changsha, China, and the Ph.D. degree from Beijing Jiaotong University, Beijing, China.

He was the Deputy Director with the Science and Technology Department, Ministry of Railways, and the President of Southwest Jiaotong University. He is currently the Vice President of Central South University. His research interests include the electric locomotive and intelligent transportation system.

Te-Fang Chen was born in Lianyuan, China, in 1957. He received the B.E. degree in automation from Dalian University of Technology, Dalian, China, in 1981, and the M.S. and Ph.D. degrees in electrical engineering from the Central South University, Changsha, China, in 1991 and 2005, respectively.

Since 1982, he has been a permanent Researcher with the Institute of Rail Transport and Electric Traction Technology. He is currently a Professor with the School of Traffic and Transportation Engineering, Central South University. His research areas include fault diagnosis and fault-tolerant control of electrical drivers and electric traction control technology.

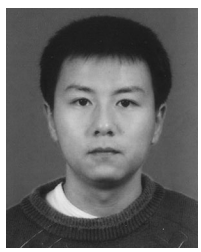

Shu Cheng was born in Changsha, China, in 1981. He received the B.E. degree in automation from East China University of Science and Technology, Shanghai, China, in 2003, and the M.S. and Ph.D. degrees in electrical engineering from the Central South University, Changsha, China, in 2006 and 2011, respectively.

Since 2007, he has been a permanent Researcher with the Institute of Rail Transport and Electric Traction Technology. He is currently an Associate Professor with the School of Traffic and Transportation Engineering, Central South University. His research interests include fault diagnosis and fault-tolerant control of electrical drivers and electric traction control technology.

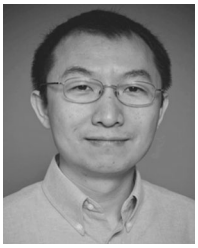

Zhi-Hong Mao (S'96–M'05–SM'09) received the dual bachelor's degrees in automatic control and mathematics and the M.Eng. degree in intelligent control and pattern recognition from Tsinghua University, Beijing, China, the S.M. degree in aeronautics and astronautics from the Massachusetts Institute of Technology, Cambridge, MA, USA, and the Ph.D. degree in medical engineering and medical physics from the Harvard-MIT Division of Health Sciences and Technology, Cambridge, MA, USA, in 1995, 1998, 2000, and 2006, respectively.

In 2005, he joined the University of Pittsburgh, Pittsburgh, PA, USA, as an Assistant Professor and became an Associate Professor in 2011 and William Kepler Whiteford Faculty Fellow in 2012.

Dr. Mao was the recipient of the CAREER Award of National Science Foundation in 2010, Andrew P. Sage Best Transactions Paper Award of the IEEE Systems, Man and Cybernetics Society in 2010, Outstanding Service Award of IEEE Transactions on Intelligent Transportation Systems in 2013, and Pitt Chancellor's Distinguished Teaching Award in 2016.

Tian-Jian Yu received the Ph.D. degree in traffic equipment and information engineering from Central South University (CSU), Changsha, China, in 2017.

Since 2014, he has been a Visiting Ph.D. Student with the University of Pittsburgh, Pittsburgh, PA, USA. He is currently a Lecturer with CSU. His research interests include fault diagnosis of traffic equipment, in particular, on bearings and inverters, by means of machine learning.

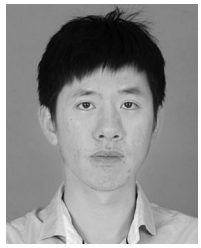

Kaidi Li was born in Nanning, China, 1992. He received the B.E. degree in electrical engineering from Changsha University of Science and Technology, Changsha, China, in 2013, and the M.S. degree in electrical engineering, in 2016, from the Central South University, Changsha, China, where he is currently working toward the Ph.D. degree in transportation engineering with the Institute of Rail Transport and Electric Traction Technology.

His research interests include fault diagnosis and fault-tolerant control of power electronic converters.